Supplementary data

Formation of Two-dimensional Metals by Weak Intermolecular Interactions Based on the Asymmetric EDO-TTF Derivatives†‡

Xiangfeng Shao *[a, c], Yoshiaki Nakano [a], Hideki Yamochi *[a, c], Alexander D. Dubrovskiy [b], Akihiro Otsuka [a], Tsuyoshi Murata [b], Yukihiro Yoshida [b], Gunzi Saito [a,b] and Shin-ya Koshihara [c,d]

[a]Research Center for Low Temperature and Materials Sciences, Kyoto University, Sakyo-ku, Kyoto 606-8502, Japan; [b]Division of Chemistry, Graduate School of Science, Kyoto University, Sakyo-ku, Kyoto 606-8502, Japan; [c]Non-equilibrium Dynamics Project, ERATO, Japan Science and Technology Agency, c/o KEK, 1-1 Oho, Tsukuba, Ibaraki, 305-0801, Japan; [d]Frontier Collaborative Research Center & Department of Materials Science, Tokyo Institute of Technology, 2-12-1 Oh-okayama, Meguro-ku, Tokyo 152-8551, Japan.

Email: yamochi@kuchem.kyoto-u.ac.jp (H. Yamochi); shao_xf@kuchem.kyoto-u.ac.jp (X. F. Shao)

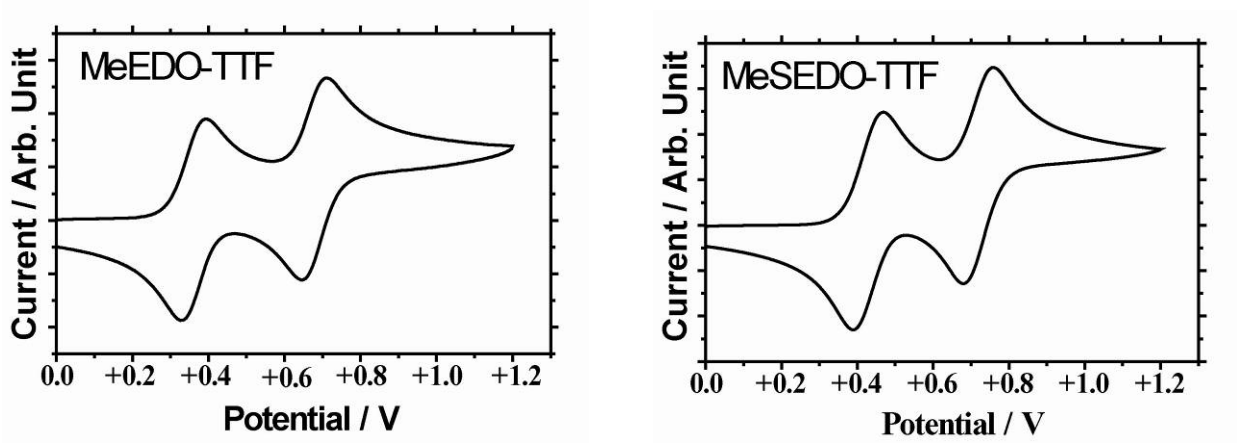

Fig. S1 Cyclic voltammograms of MeEDO-TTF and MeSEDO-TTF. The measurement was carried out in the solution of 0.1 mol L^{-1} $(Bu_4N)BF_4$ in CH_3CN at room temperature.

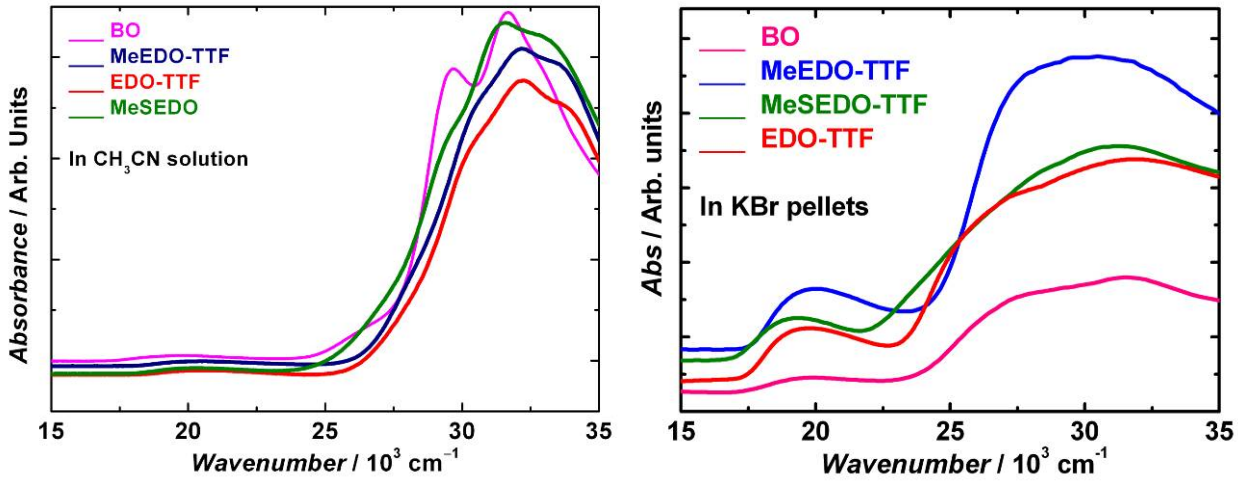

Fig. S2 Optical absorption spectra of MeEDO-TTF and MeSEDO-TTF in CH_3CN (left panel) and dispersed in KBr (right panel). The spectra were compared with those of EDO-TTF and BO.

Table S1 Experimental condition for the preparation of cation radical salts.

salts	donor, mg	supporting electrolytes, mg	solvent, mL	current, μA	yield, mg
7	10.3	$(Bu_4N)BF_4$, 95.6	EtOH, 17	0.5	7.8
8	9.7	$(Bu_4N)ClO_4$, 93.4	EtOH, 17	0.5	6.5
9	10.5	$(Bu_4N)PF_6$, 98.3	EtOH, 17	0.5	6.1
10	8.7	$(Bu_4N)AsF_6$, 97.2	EtOH, 17	0.5	5.4
11	9.4	$(Bu_4N)SbF_6$, 95.4	EtOH, 17	0.5	6.2
12	10.1	$(Bu_4N)_2$(HCTMM), 68.9	EtOH, 17	0.5	4.7
13	10.2	$(Bu_4N)PF_6$, 96.6	EtOH, 17	0.5	6.9
14	10.6	$(Bu_4N)AsF_6$, 97.2	EtOH, 17	0.5	7.1
15	9.6	$(Bu_4N)SbF_6$, 98.2	EtOH, 17	0.5	5.3
16	9.3	$(Bu_4N)_2$(HCTMM), 72.4	EtOH, 17	0.5	5.2

The supporting electrolytes were recrystallized from appropriate solvent. EtOH was distilled over Mg/I_2 under the protection of nitrogen gas. After distillation, it was stored in the long-necked flask under nitrogen atmosphere. The electrocrystallization was carried out at room temperature by applying constant current. After around two weeks, the cation radical salts were obtained as black powder or thin plates.

For MeSEDO-TTF, the electrocrystallization of the donor in the presence of $(Bu_4N)BF_4$, $(Bu_4N)ClO_4$, or $(Bu_4N)ReO_4$ didn't afford the solid cation radical salts.

Table S2 The results of elemental analyses for the MeEDO-TTF and MeSEDO-TTF cation radical salts.

Anion (A)	MeEDO-TTF (D)				MeSEDO-TTF (D)			
	Entry	D : A	Found (%)	Calc. (%)	Entry	D : A	Found (%)	Calc. (%)
BF_4	7	2 : 1	C: 33.94 H: 2.76	C: 33.80 H: 2.52				
ClO_4	8	2 : 1	C: 33.26 H: 2.52 Cl: 5.36	C: 33.14 H: 2.47 Cl: 5.44				
PF_6	9	2 : 1	C: 31.04 H: 2.45 F: 16.17	C: 30.98 H: 2.31 F: 16.34	13	2 : 1	C: 28.38 H: 2.15 F: 14.78	C: 28.37 H: 2.12 F: 14.96
AsF_6	10	2 : 1	C: 28.88 H: 2.15 F: 15.46	C: 29.15 H: 2.17 F: 15.37	14	2 : 1	C: 26.55 H: 1.99 F: 14.12	C: 26.83 H: 2.00 F: 14.14
SbF_6	11	2 : 1	C: 27.68 H: 2.04	C: 27.42 H: 2.05	15	2 : 1	C: 25.51 H: 1.82	C: 25.35 H: 1.89
HCTMM	12	4 : 1	C: 41.97 H: 2.56 O: 10.00 S: 39.28 N: 6.38	C: 42.10 H: 2.46 O: 9.77 S: 39.17 N: 6.42	16	13 : 3	C: 38.02 H: 2.21 O: 9.30 S: 44.94 N: 5.23	C: 38.19 H: 2.27 O: 9.00 S: 45.09 N: 5.45

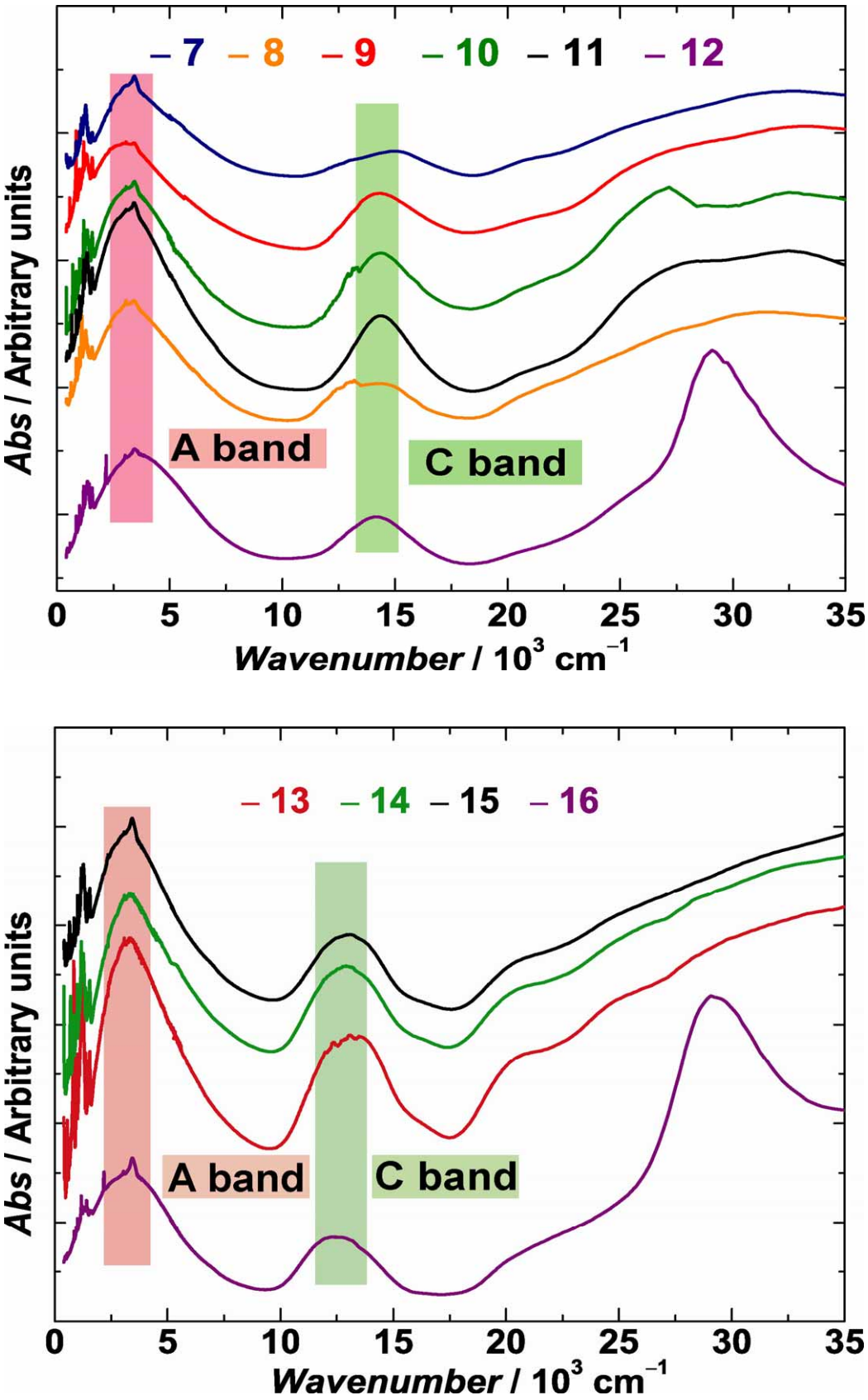

Fig. S3 Optical absorption spectra of all of the cation radical salts. The spectra were measured on KBr pellets.

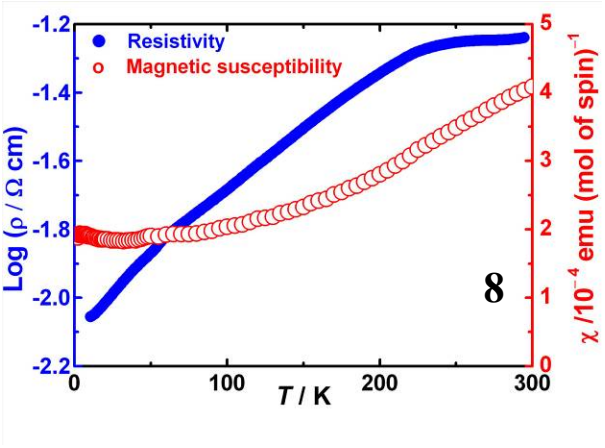
Resistivity
Magnetic susceptibility
8
Log (ρ / Ω cm)
χ /10⁻⁴ emu (mol of spin)⁻¹
T / K

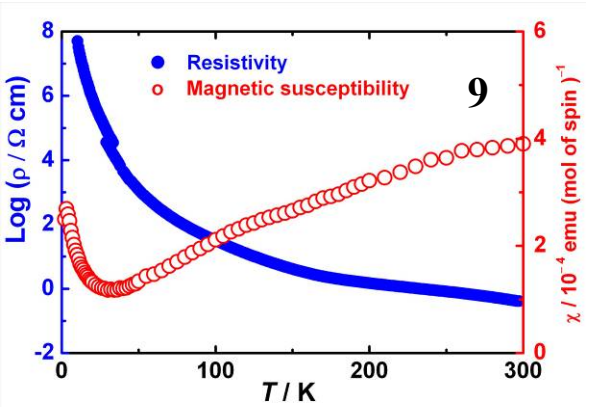
Resistivity
Magnetic susceptibility
9
Log (ρ / Ω cm)
χ / 10⁻⁴ emu (mol of spin)⁻¹
T / K

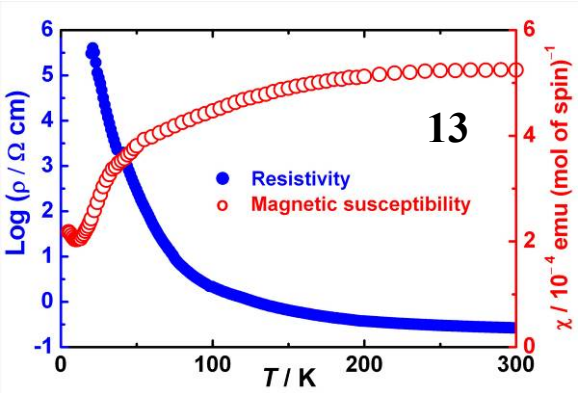
Resistivity
Magnetic susceptibility
13
Log (ρ / Ω cm)
χ / 10⁻⁴ emu (mol of spin)⁻¹
T / K

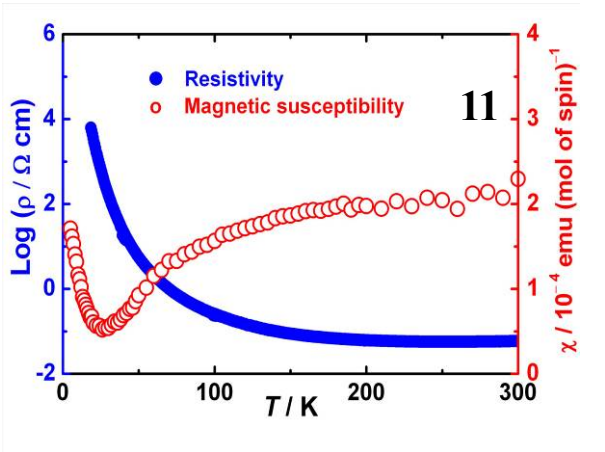
Resistivity
Magnetic susceptibility
11
Log (ρ / Ω cm)
χ / 10⁻⁴ emu (mol of spin)⁻¹
T / K

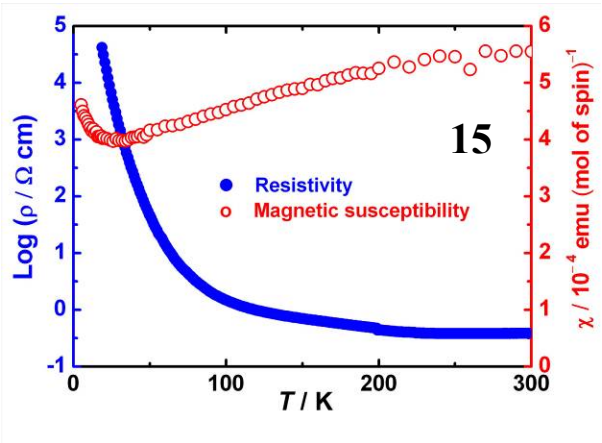
Resistivity
Magnetic susceptibility
15
Log (ρ / Ω cm)
χ / 10⁻⁴ emu (mol of spin)⁻¹
T / K

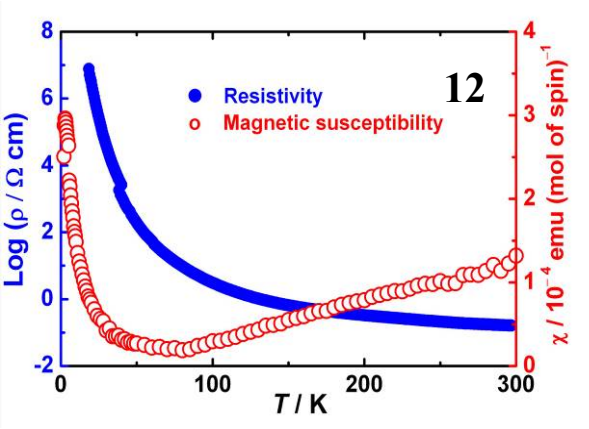
Resistivity
Magnetic susceptibility
12
Log (ρ / Ω cm)
χ / 10⁻⁴ emu (mol of spin)⁻¹
T / K

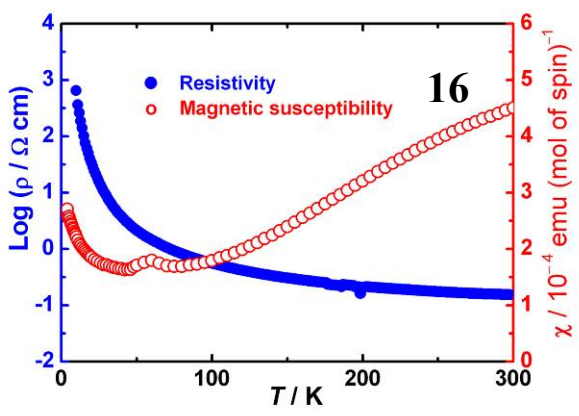
Resistivity
Magnetic susceptibility
16
Log (ρ / Ω cm)
χ / 10⁻⁴ emu (mol of spin)⁻¹
T / K

Fig. S4 Temperature dependent resistivity (ρ: blue closed circle) and static susceptibility (χ: red open circle) of cation radical salts. The entry number of the salt is indicated in each panel. The left and right axes in each panel indicate log (ρ) and χ, respectively. The disconnections of the log(ρ)–T plots were due to the changing of the techniques of four- and two-probe methods at around 40 K.
The magnetic susceptibility was measured by using polycrystalline sample, under a field of 10 kOe. For the salts of **11**, **12**, and **15**, the scattered data at high temperature region were due to the instability of the temperature control system of the SQUID magnetometer. All of the magnetic susceptibilities in these figures were the data after substracting the core diamagnetism term and Curie impurities.

$$\chi = \chi_{obs} - \chi_{dia} - \frac{C}{T}$$

χ_{obs}: Experimental data

χ_{dia}: Core diamagnetism, which is calculated from a tabulation of Pascal's constants

C: Curie constant in the unit of 10^{-4} emu K (mol of spin)$^{-1}$.

T: Temperature in the unit of K

Table S3 The calculated core diamagnetism and Curie constant for each cation radical salt

Entry	χ_{dia} / 10^{-4} emu mol^{-1}	C / 10^{-4} emu K (mol of spin)$^{-1}$	Entry	χ_{dia} / 10^{-4} emu mol^{-1}	C / 10^{-4} emu K (mol of spin)$^{-1}$
7	-2.988	0.681			
8	-2.938	0.581			
9	-3.268	8.751	**13**	-3.568	30.821
10	-3.318	14.633	**14**	-3.618	27.127
11	-3.398	19.732	**15**	-3.698	16.274
12	-3.015	36.323	**16**	-3.551	24.4

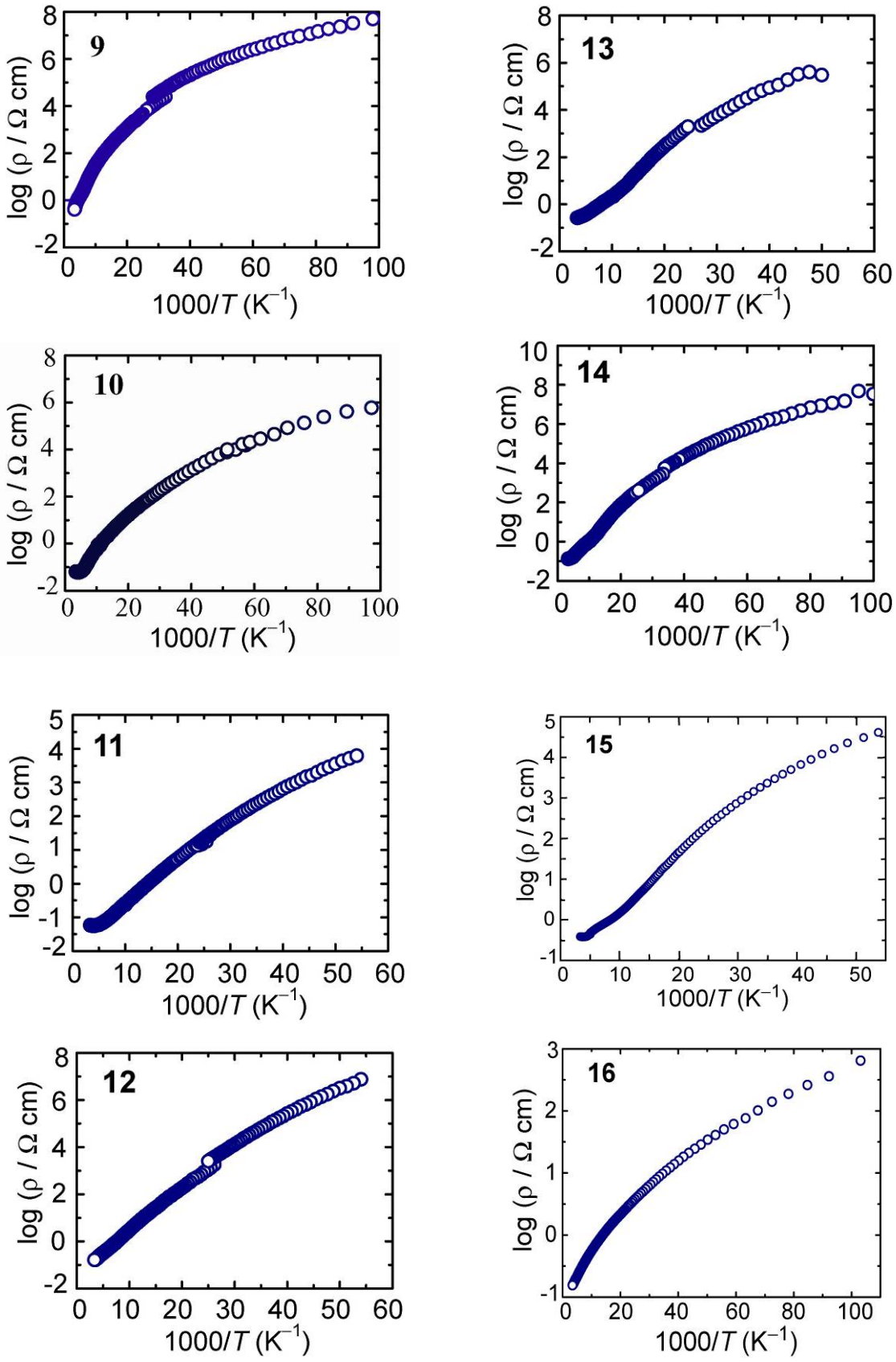

Fig. S5 Arrhenius plots ($\log(\rho)$–T^{-1}) for the temperature dependent resistivities of the radical cation salts in this investigation other than the stable metallic salts **7** and **8**. The disconnections of the $\log(\rho)$–T^{-1} plots were due to the changing of the techniques of four- and two-probe methods at around 40 K.

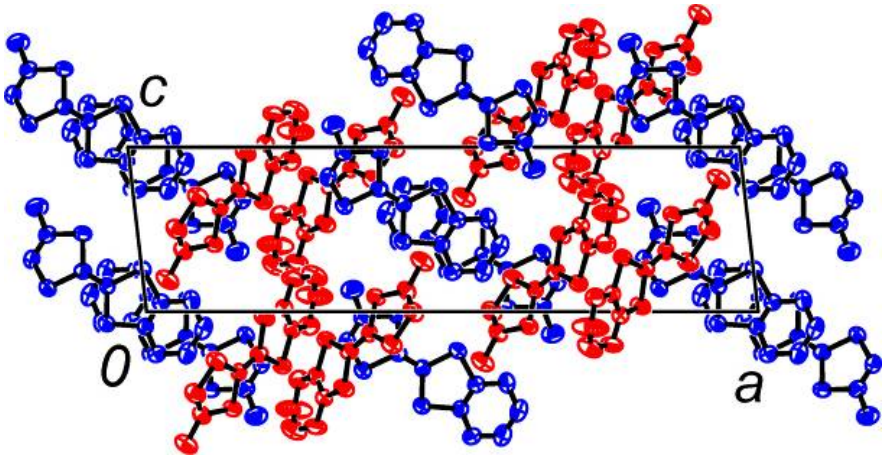

Fig. S6 Crystal structure of MeEDO-TTF (**2**) projected along *b*-axis (ORTEP plot with 50% probability). The crystallographically independent molecules **A** and **B** were painted in red and blue, respectively. The hydrogen atoms were omitted for clarity.

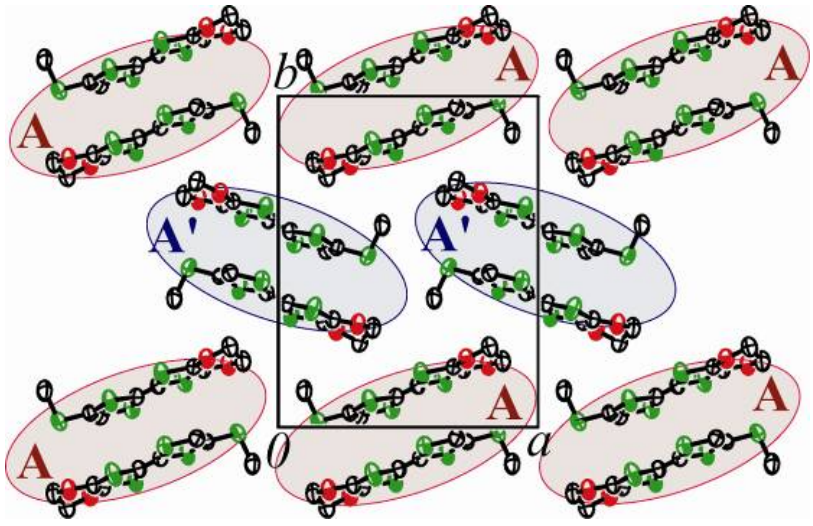

Fig. S7 Crystal structure of MeSEDO-TTF (**3**) projected along the *c*-axis (ORTEP plot with 50% probability). Only the molecules located at $z = 1/2$ were depicted, while those at $z = 0$ were drawn in Fig. 4.

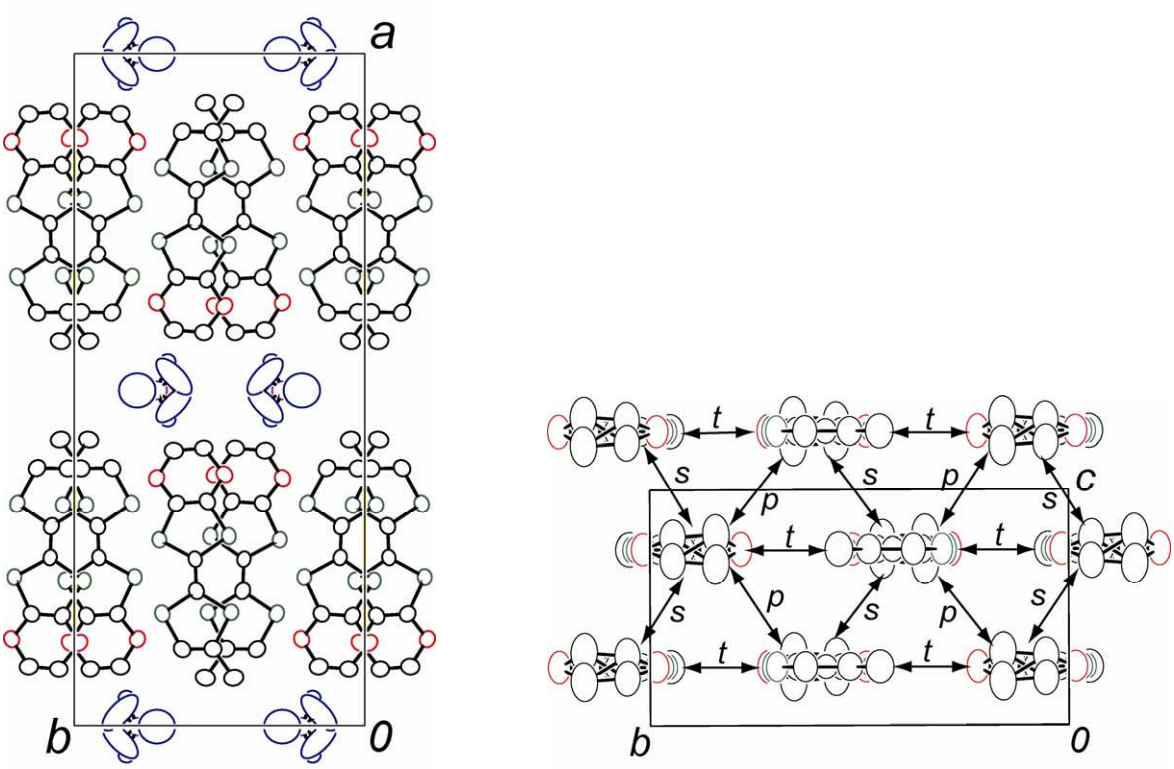

(a) **(b)**

Fig. S8 Crystal structure of **8** (ORTEP plot with 50% probability): (a) Projection of the structure on the *ab*-plane; (b) View of the donor layer along the *a*-axis with scheme of the intermolecular overlap integrals. The hydrogen atoms are omitted for clarity. $t = 11.3$, $p = 8.5$, $s = -5.4 \times 10^{-3}$

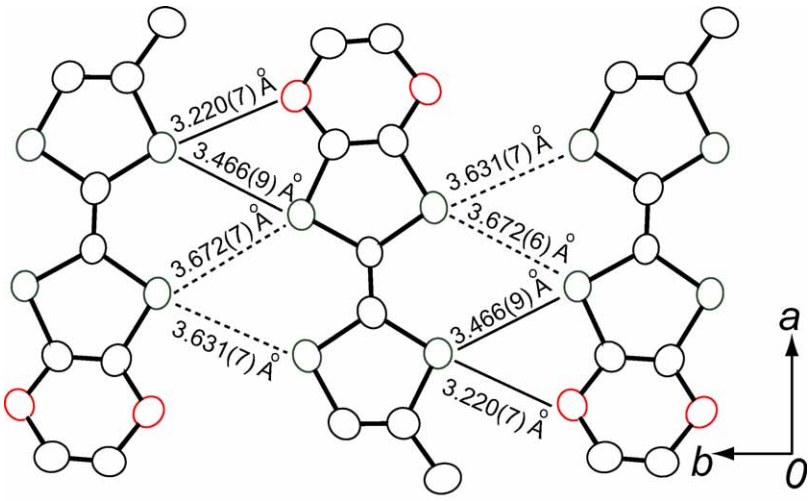

Fig. S9 Intermolecular side-by-side contacts in **8** (ORTEP plot with 50% probability). Solid lines indicate the S···S and S···O contacts shorter than the sum of van der Waals radii (< 3.60 and < 3.45 Å, respectively), while the dashed lines show those slightly longer than the sum of van der Waals radii.

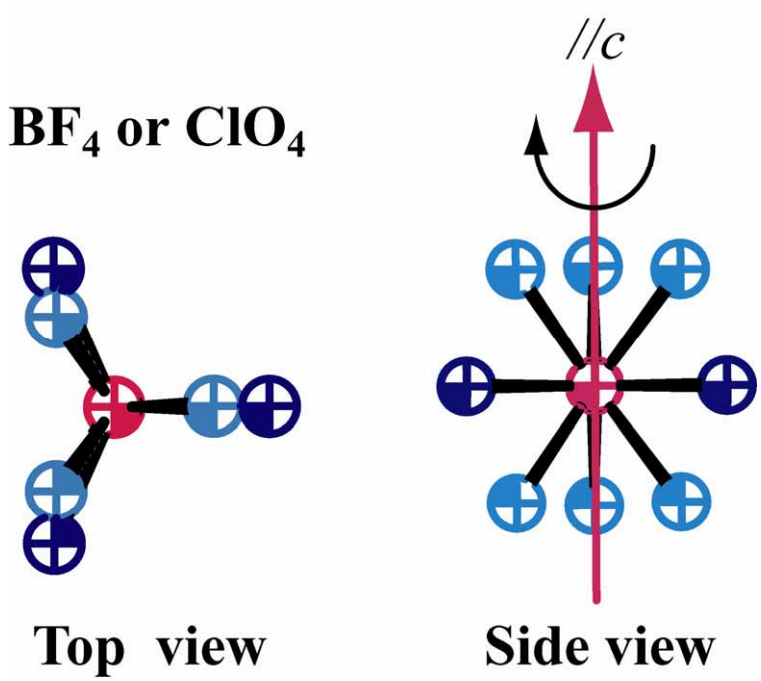

Fig. S10 The pseudo-three-fold rotational disorder of the anion in $(MeEDO\text{-}TTF)_2BF_4$ (**7**). Red and navy colored spheres indicate the positions of boron and fluorine atoms on a crystallographic mirror plane at z = 1/4, respectively. The cyan spheres show the positions of other fluorine atoms. Top view corresponds to the projection onto the mirror plane at z = 1/4. In the side view, the red arrow corresponds to the non-crystallographic pseudo-three-fold axis of rotation parallel to the c-axis. The equator of this rotational disorder lies on the mirror plane at z = 1/4. This description is valid also for ClO_4 salt (**8**) when the atom names of boron and fluorine are replaced by chlorine and oxygen, respectively.

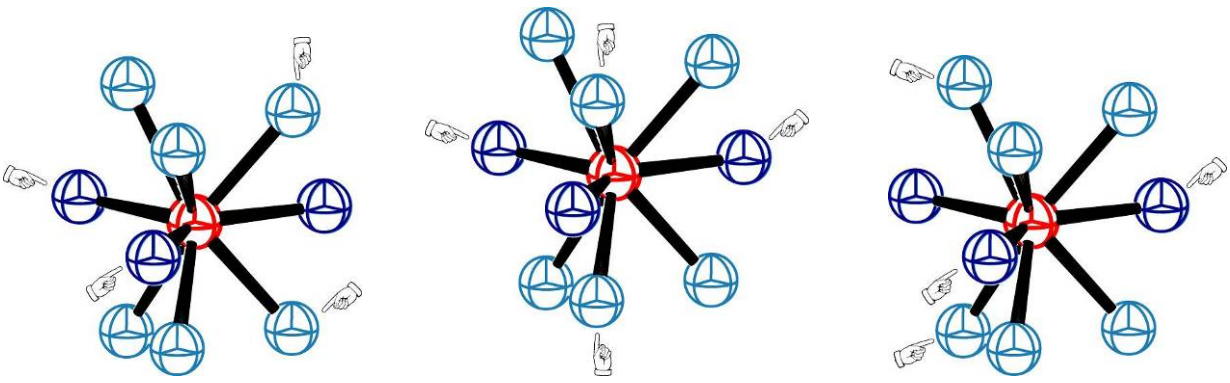

Fig. S11 The choice of atomic sites to construct a tetrahedral anion (BF_4 or ClO_4). The color of each sphere corresponds to that in Fig. S10. To construct a tetrahedron around the central atom painted in red, each two sites on and out of the equator are chosen as indicated by forefingers. Three sets of choices are possible as shown here.

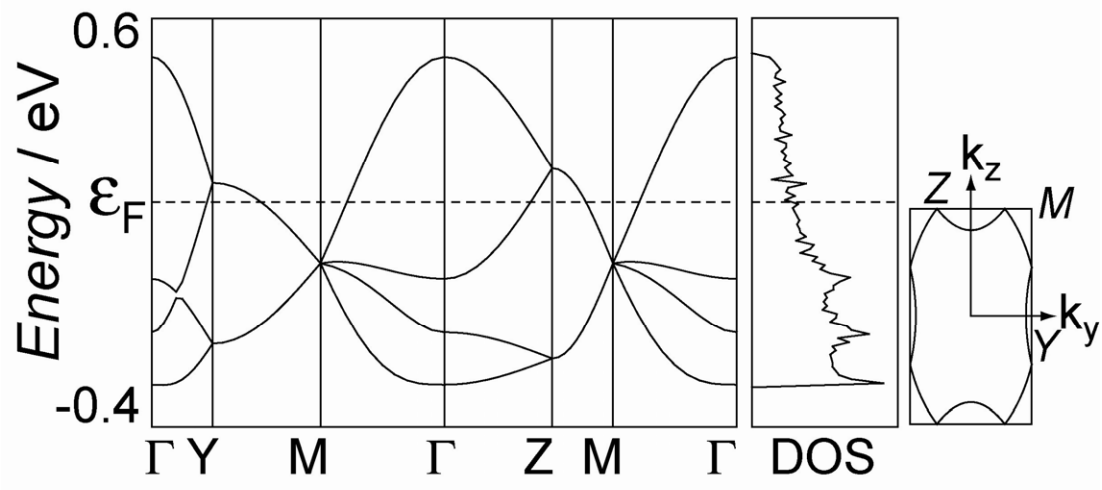

Fig. S12 Calculated energy dispersion, density of states (DOS), and Fermi surface of salt **8**.

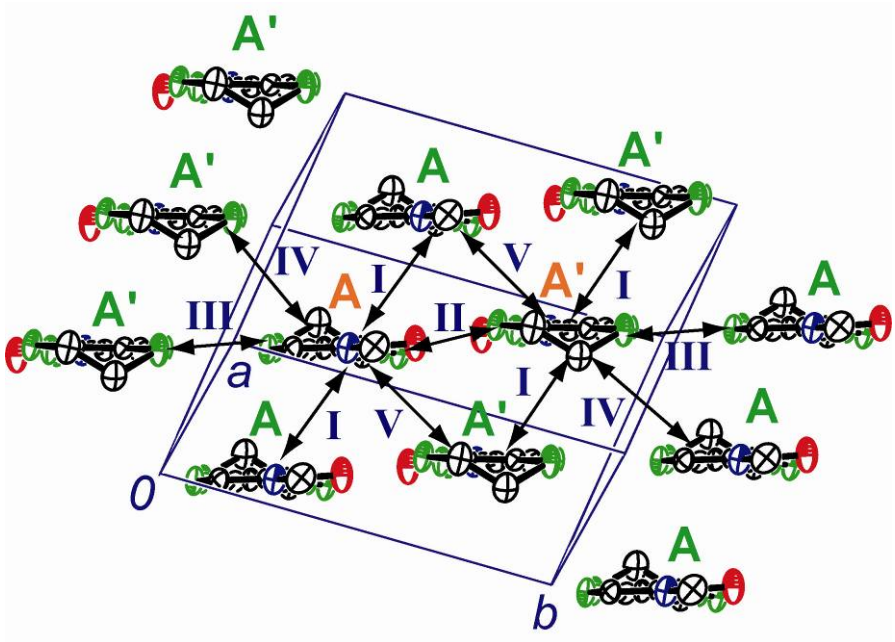

Fig. S13 The donor layer of $(EDT\text{-}TTF\text{-}CONHMe)_2(Cl{\bullet}H_2O)$ viewed along the molecular longitudinal axis with scheme of the intermolecular overlap integrals (ortep plot with 50% probability). The atomic coordinates were taken from the supporting information of ref. 23. **A** indicates the crystallographically independent molecule, while **A′** is derived from **A** by the symmetry operation (1-*x*, 1-*y*, 1-*z*). Intermolecular overlap integrals, **I** = 10.9, **II** = −6.8, **III** = −11.4, **IV** = 8.6, and **V** = 15.9×10^{-3}, were obtained by using the same parameters for atomic orbitals to those applied in the calculations for **7** and **8**.